# Investigation of mass and energy coupling between soot particles and gas species in modelling counterflow diffusion flames

# INVESTIGATION OF MASS AND ENERGY COUPLING BETWEEN SOOT PARTICLES AND GAS SPECIES IN MODELLING COUNTERFLOW DIFFUSION FLAMES

L. Zimmer[a,*], F. M. Pereira[a], J. van Oijen[b], P. de Goey[b]

[a]*Mechanical Engineering Department, Federal University of Rio Grande do Sul, Rua Sarmento Leite, n. 425, Porto Alegre, Brazil*
[b]*Combustion Technology, Mechanical Engineering, Eindhoven University of Technology, 5600 MB Eindhoven, The Netherlands*

**Abstract**

A numerical model is developed aiming at investigating soot formation in ethylene counterflow diffusion flames at atmospheric pressure. In order to assess modeling limitations the mass and energy coupling between soot solid particles and gas-phase species are investigated in detail. A semi-empirical two equation model based on acetylene as the soot precursor is chosen for predicting soot mass fraction and number density. For the solid-phase the model describes particle nucleation, surface growth and oxidation. For the gas-phase a detailed kinetic mechanism is considered. Additionally, the effect of considering gas and soot radiation heat losses is evaluated in the optically thin limit approximation. The results show that for soot volume fractions higher than a certain threshold value the formation of the solid particles begins to significantly influence the gas-phase composition and temperature. The results also show that the inclusion of radiant heat losses decreases this influence.

*Keywords:* Combustion, Soot model, Coupling effect, Counterflow flames

## Introduction

Soot is commonly found in diffusion flames of hydrocarbon fuels. The presence of soot particles increases the radiant heat losses, decreases the flame temperature and gives a characteristic yellowish luminosity to the flame. The increased radiant heat transfer is not desirable for devices such as gas turbines and diesel engines due to a decrease of the device performance, but may be of interest in industrial furnaces where high heat transfer rates are required. In flares of petrochemical plants or off-shore platforms the presence of soot influences the intensity of the radiant heat flux at the ground level which determines the minimum stack hight to protect personnel and equipment. In all cases, emissions of soot particles to the atmosphere are limited by law due to environmental and health concerns. Therefore, the capability of predicting soot formation in flames is important for a large range of applications.

The physics of soot formation is not yet fully understood [1], but significant progress has been made and now it is possible to model many steps involved in the process. In [2] the models for soot prediction are grouped in three categories: (i) empirical correlations, (ii) semi-empirical models and (iii) models with detailed chemistry. In the first category, models rely on global rate equations for soot generation and destruction adjusted to reproduce experimental data in specific combustion devices. They are easy to implement and are computationally fast, but since they do not describe soot formation steps, their validity is restricted to the conditions and devices for which they were developed. In the second category, the models attempt to incorporate some fundamental steps of the soot formation process, i. e., precursor formation, soot inception, particle growth, coagulation and oxidation. The rate equations are still dependent on the experimental conditions used to fit the model, but they are not dependent on specific devices. The balance equations for the solid-phase may consider a single particle size or a distribution of particle sizes (for example, dividing the solid-phase in a certain number of sections with characteristic sizes with one balance equation for each section). Radiation heat losses may also be accounted for by including gas and particle emissions. Thus, many options can be chosen depending on the goals of the study. The general idea is that these models can give more detailed results with a reasonable computational cost. In the third category, the models are improved with detailed kinetic mechanisms. Different species, in general PAHs, may be involved in the nucleation process and can be considered as soot precursors. Similarly, different species may participate in the particle surface growth process. Thus, detailed gas-phase kinetic mechanisms are required to model these species formation and consumption as well as their interaction with the particle surface. The validation of such mechanisms is still a challenge and there is no consensus in the literature on which species should be included. In this category the distribution of particle

*Corresponding author
*Email address:* leo.zimmer@mecanica.ufrgs.br (L. Zimmer)

sizes is usually taken into account by statistical models based on particle population balance equations for particle distribution. Since models in this category are more fundamental, they are likely to work in different combustion situations, although, as any kinetic mechanism a dependence on experiments remains since the reaction rate parameters are not derived from first principles. The drawback of this approach is the difficult implementation and high computational costs.

Soot nucleation, growth and oxidation implies the consumption and formation of some gas-phase species. On the other hand, the presence of soot particles implies additional energy source terms. When modeling sooting flames one has to decide how these interactions should be accounted for. Some models neglect the mass and energy coupling between gas and solid phases ([3], [4]) considering that the amount of soot within the flame is so small that it does not alter the flame composition and enthalpy. Other models include the coupling terms ([5–8]) although the importance of this choice is not clear.

Carbonell *et al.* [9] studied a laminar coflow diffusion flame employing different implementations of a flamelet approach including coupled and non-coupled versions. They chose the Leung model [10] for soot prediction based on acetylene as the soot precursor. Their results showed that the non-coupled version over-predicts soot formation. This happened because there was an excess of $C_2H_2$ in the flame which increases soot nucleation and growth. The authors conclude that considering the coupling was important, but they didn't explore their model in different conditions. Then, the question that remains is what are the conditions for which a full description of the gas- and solid-phase interactions is mandatory.

In this paper the mass and energy coupling between the soot particles and the gas-phase species is investigated for sooting ethylene counterflow flames using an existing semi-empirical model. In order to determine whether the coupling effect is important the model is explored in conditions that produce low and high amounts of soot. Adiabatic and non-adiabatic (with radiation) situations are also investigated.

## Numerical models

Combustion problems are modeled with a set of partial differential equations that describe conservation of total mass, mass of species, momentum, and energy. For counter-flow flames a one-dimensional approximation can be employed. The derivation of this set of equations can be found in [11] and will not be repeated here. Details of the soot model implementation are given in the following sections.

### *Soot model*

The soot model used in this work is based on [5, 10]. This model is a semi-empirical acetylene based model that describes soot particle nucleation, surface growth and oxidation. Two additional equations are included in the system of conservation equations, one for soot mass fraction, $Y_S$, and another for soot number density, $N_S$ ($particles/kg\ of\ mixture$). These two equations for an one-dimension planar stagnation flow are shown below.

$$\frac{\partial(\rho Y_S)}{\partial t} + \frac{\partial(\rho u Y_S)}{\partial x} = -\frac{\partial(\rho V_T Y_S)}{\partial x} + \frac{\partial}{\partial x}\left(\rho D_p \frac{\partial Y_S}{\partial x}\right) + \dot{w}''_{Y_S} - \rho K Y_S, \quad (1)$$

$$\frac{\partial(\rho N_S)}{\partial t} + \frac{\partial(\rho u N_S)}{\partial x} = -\frac{\partial(\rho V_T N_S)}{\partial x} + \frac{\partial}{\partial x}\left(\rho D_p \frac{\partial N_S}{\partial x}\right) + \dot{w}''_{N_S} - \rho K N_S, \quad (2)$$

where $\rho$ is the mixture density ($kg/m^3$), $u$ is the fluid velocity ($m/s$), $V_T$ is the thermophoretic velocity of the soot particles ($m/s$), $D_p$ the soot diffusion coefficient ($m^2/s$), $\dot{w}''_{Y_S}$ and $\dot{w}''_{N_S}$ are the source terms of soot mass fraction ($kg/m^3 s$) and soot density number ($particles/m^3.s$), respectively, and $K$ the stretch rate ($s^{-1}$). The stretch rate $K$ accounts for the deviations from the one-dimensional condition [11]. Many researches [1, 5, 10, 12, 13] neglect the Brownian motion of soot particles, since soot transport is usually dominated by convective and thermophoretic effects. A small soot diffusion term is retained in this work to enhance numerical stability. In the same manner as [14], who used a soot diffusivity of 1% of the gas diffusivity, the value of $D_p$ here is set as $1 \times 10^{-6}\ m^2/s$. The thermophoretic velocity of soot, $V_T$, is modeled as:

$$V_T = -0.50 \frac{\mu}{\rho} \frac{1}{T} \frac{\partial T}{\partial x}. \quad (3)$$

where $\mu$ is the mixture dynamic viscosity ($kg/m.s$) and $T$ is the mixture temperature ($K$).

The source terms for Eqs. 1 and 2 are:

$$\dot{w}''_{Y_S} = M_S\,(2R_1 + 2R_2 - R_3 - R_4 - R_5), \quad (4)$$

$$\dot{w}''_{N_S} = \frac{2}{C_{min}} N_A R_1, \quad (5)$$

where $R_1$, $R_2$, $R_3$, $R_4$ and $R_5$ are soot particle nucleation, surface growth, oxidation by $O_2$, $OH$ and oxidation by $O$ process rates, respectively. $M_S = 12.011$ ($kg/kmol$) is the soot molar mass, based on carbon element, $C_{min} = 700$ is the number of carbon atoms in the incipient soot particle and $N_A = 6.022 \times 10^{26}$ ($particles/kmol$) is the Avogadro's number.

Equation 4 takes into account soot particle nucleation, surface growth and oxidation by $O_2$, $OH$ and $O$ radicals. In this model the nucleation of the first particle follows the acetylene path, therefore the nucleation reaction depends on the acetylene concentration only as $C_2H_2 \rightarrow 2C_S + H_2$, where $C_S$ is solid carbon. The surface growth is modelled as $C_2H_2 + nC_S \rightarrow$

$(n+2)\,C_S + H_2$. The nucleation rate $R_1$ $(kmol/m^3 s)$ is written as $R_1 = k_1(T)[C_2H_2]$ and surface growth rate $R_2$ $(kmol/m^3 s)$ is written as $R_2 = k_2(T)f(S)[C_2H_2]$ where $f(S)$ is the function which expresses the dependence of the surface growth term on soot surface area. In this model $f(S) = \sqrt{S}$. The surface area $S$ $(m^2)$ can be defined as $S = \pi d_p^2\,(\rho N_S)$ and $d_p = (6Y_S/\pi\rho_C N_S)^{1/3}$, where $d_p$ $(m)$ is the soot particle diameter and $\rho_C = 1,900$ $(kg/m^3)$ is the soot density. The oxidation by $O_2$ is based on the NSC model [15] for which oxygen reacts at the particle surface as $C_S + {}^1/_2O_2 \rightarrow CO$ and the oxidation rate is $R_3 = k_3 S$, where the oxidation rate constant $k_3$ is taken from [15]. The oxidation by the $OH$ radical follows $C_S + OH \rightarrow CO + H$ and the oxidation rate $R_4$ $(kmol/m^3 s)$ is written as $R_4 = k_4(T)S$, where the rate constant $k_4$ is taken from [3]. The oxidation by the $O$ radical follows $C_S + O \rightarrow CO$ and the oxidation rate $R_5$ $(kmol/m^3 s)$ is written as $R_5 = k_5(T)S$, where the rate constant $k_5$ is taken from [16].

Equation 5 takes into account the production of particles by soot nucleation only. In [17] it is suggested that the destruction of particles by coagulation is negligible and based on recommendations made by [1] was neglected.

*Radiation model*

The radiant heat losses are modelled by using the grey-gas approximation, i.e., there is no dependence on the wave number, and the optical thin limit, i.e., the medium does not scatter nor absorb radiation. Then, the heat source in the energy conservation equation due to radiant heat losses [18] is :

$$q_R^{'''} = -4\sigma\kappa(T^4 - T_\infty^4) - C f_v T^5, \tag{6}$$

$$\kappa = \sum p_i \kappa_i, \tag{7}$$

where $\sigma$ is the Stefan-Boltzmann constant, and $T_\infty$ is the ambient temperature. $\kappa$ denotes the Planck mean absorption coefficient of the mixture, and $p_i$ and $\kappa_i$ are respectively the partial pressure and Planck mean absorption coefficient of species $i$, given in [19]. The participant gas species are $H_2O$, $CO_2$, $CO$ and $CH_4$. $C = 4.243 \times 10^{-4}$ $(W/m^3)$ is a constant taken from [20] and $f_v = \rho Y_S/\rho_C$ $(m^3/m^3)$ is the soot volume fraction.

*Two-way coupling of soot and gas species*

It is assumed that the solid phase is diluted and it is an additional gas species, the $(N+1)th$ species in the mixture $(Y_{N+1} = Y_S)$. The interaction between the soot chemistry and the gas-phase chemistry was accounted for in the conservation equations of total mass, species transport and energy. This means that additional source terms for species related to soot formation and oxidation ($C_2H_2$, $H_2$, $CO$, $H$, $O_2$, $OH$ and $O$) are added to the system of equations. Thus, the elements are conserved, the summation of species mass fraction is equal to one $(\sum_{i=1}^{N+1} Y_i = 1)$ and the summation of species source terms (mass basis) is equal to zero $(\sum_{i=1}^{N+1} \dot{w}_i^{''} = 0)$. Soot additional terms in enthalpy and heat capacity are added as $h = \sum_{i=1}^{N+1} Y_i h_i$ and $c_p = \sum_{i=1}^{N+1} Y_i c_{p_i}$. The thermodynamics properties for soot ($h_i$ and $c_{p_i}$) are approximated using the properties of solid carbon (graphite) and the data are taken from the NIST-JANAF database [21]. For simplicity it is assumed that soot does not affect the mixture viscosity and thermal conductivity of the mixture. An additional term in the energy flux formulation due to the soot thermophoretic diffusion flux, the $(N+1)th$ species, is added:

$$\vec{j_q} = -\lambda\vec{\nabla}T + \sum_{i=1}^{N+1} h_i \vec{j_i}. \tag{8}$$

where, $\vec{j_i}$ is the $i$ species diffusion flux. The mixture density is calculated using the equation of state:

$$\rho = \frac{p_a MW}{\overline{R}T}, \quad MW = \left(\sum_{i=1}^{N} \frac{Y_i}{MW_i}\right)^{-1}. \tag{9}$$

where $\overline{R}$ is the universal gas constant, $MW$ the mixture molar mass, $Y_i$ is $i$ species mass fraction and $MW_i$ the $i$ species molar mass.

*Reacting flow code*

The system of equations is solved using a specialized flame code CHEM1D (a code for solving one-dimensional flames developed at the Eindhoven Technological University)[22]. The chemical kinetic mechanism used was the GRI3.0, the diffusion coefficients are calculated through the mixture-average approach in which the diffusion velocity of each individual gas species is computed assuming Fick-like diffusion, viscosity is calculated through Wilke's approximation [23] and thermal conductivity is calculated through combination-averaging approach of Marthur [24]. An assessment of the current model was done and the results of three adiabatic cases were compared against the numerical work of Liu *et al.* [5]. Fig. 1 shows the comparison of soot volume fraction predicted by both models for three levels of oxygen concentration at the oxidant stream. The results were in good agreement and the small differences observed are due to the different reacting flow codes that were used.

## Results and Discussion

Numerical simulations were conducted under four different conditions. Two simulations were adiabatic and two were non-adiabatic. Within each heat loss condition two different cases were tested. In the first case, here called "coupled", the gas-phase chemistry is influenced by the soot formation and oxidation, with the additional terms presented above. The second case, here called "non-coupled", the gas-phase chemistry is not influenced by the soot formation and oxidation. Simulations were done to test the limits of the coupling effect

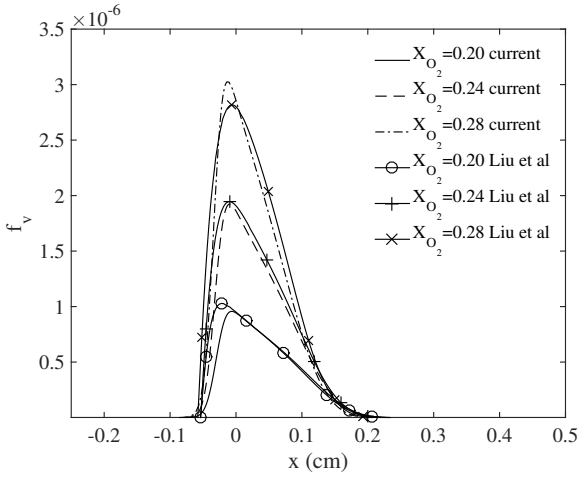


Figure 1: Comparison between the current model and Liu *et al.* [5] for three levels of $X_{O_2}$

on the soot model for ethylene/air counterflow flames. To explore a range of soot volume fractions, the strain rate, $a$, applied at the oxidizer side, is varied from 100 to 10 $s^{-1}$. The fuel stream is $X_{C_2H_4} = 1.00$ and the oxidizer stream is dry air, $X_{O_2} = 0.21$ and $X_{N_2} = 0.79$.

The flame structure for a strain rate equal to 100 $s^{-1}$ for the coupled and adiabatic case is presented in Figure 2. In this figure the species related to soot production and oxidation and the temperature profile in the physical space are presented . The fuel stream comes from the left side and the oxidiser stream comes from right side. The gas stagnation plane is located at the position $x = 0$ *cm* and the reaction zone is located in the oxidiser side. The soot is formed, through the reactions of nucleation and surface growth, in the area where high temperatures and high acetylene concentrations are found - see Figure 3.

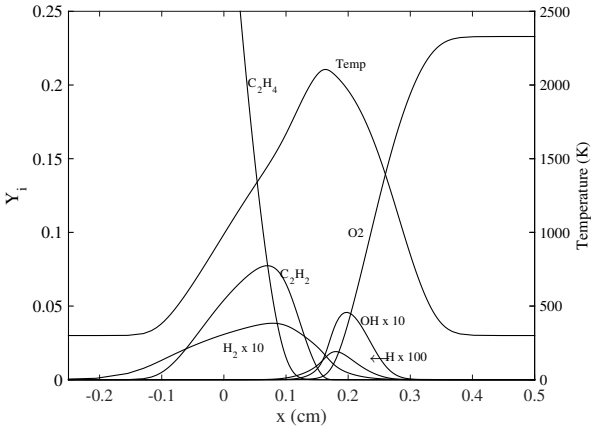


Figure 2: Flame structure for strain rate of 100 $s^{-1}$ for coupled, adiabatic case

In Fig. 3 it is seen that for this condition the maximum soot mass fraction is 0.0014 (0.247 ppm), which means that the change in the gas-phase composition is very low. Nevertheless, when the interactions between the two phases are considered, it is expected that as the

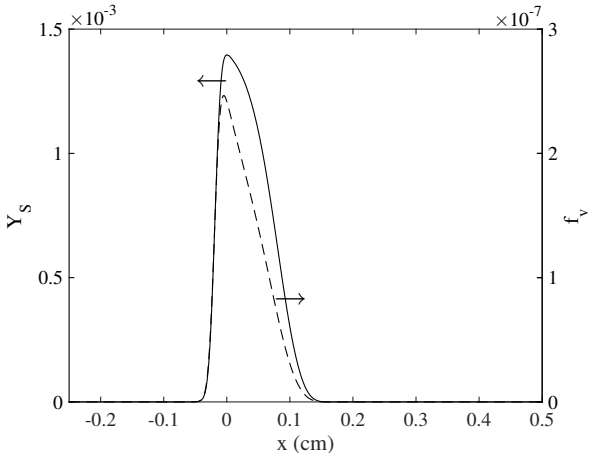


Figure 3: Soot mass fraction and volume fraction for strain rate of 100 $s^{-1}$ for coupled, adiabatic case

amount of soot increases, the species related to soot formation and oxidation, i.e. $C_2H_2$, $H_2$, $CO$, $H$, $O_2$, $OH$ and $O$, may change appreciably. Higher amounts of soot are produced at low strain rates due to the large residence times of particles in such flames.

The results for the maximum temperature, maximum soot mass fraction and maximum soot volume fractions for a range of strain rates are presented in Fig. 4, 5 and 6, respectively.

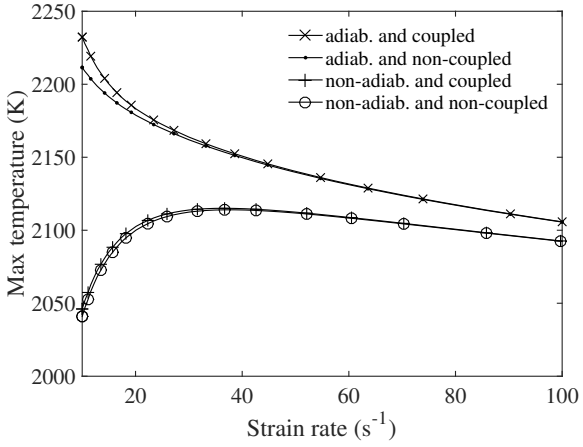


Figure 4: Maximum temperature for different strain rates

From Fig. 4 it is possible to see that as the strain rate is decreased the interaction between the two phases starts to have an effect. For the adiabatic case the difference in the temperature starts to be seen around 30 $s^{-1}$ ($Y_S = 0.01$ (Fig. 5)), it increases as the amount of soot increases (see Fig. 5), and for the lower strain rate of 10 $s^{-1}$, the temperature difference reaches $\Delta T = 20K$, a difference of 0.9%. For the non-adiabatic cases the difference in the temperature starts to be seen also around 30 $s^{-1}$, ($Y_S = 0.007$ (Fig. 5)) and for the lower strain rate of 10 $s^{-1}$, the temperature difference reaches $\Delta T = 5\ K$, a difference of 0.2%.

From Fig. 5 it is possible to see that for soot mass fraction there is no visible difference if the interaction

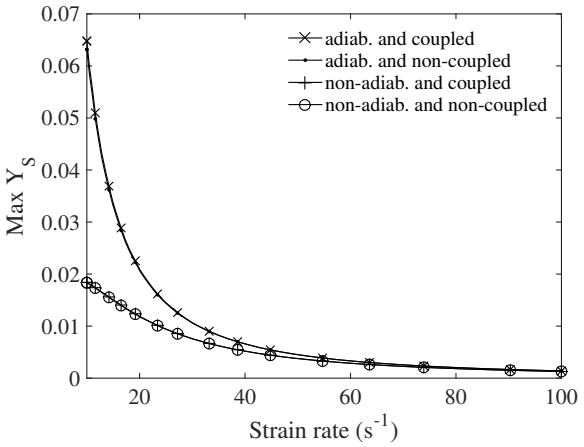


Figure 5: Maximum soot mass fraction for different strain rates

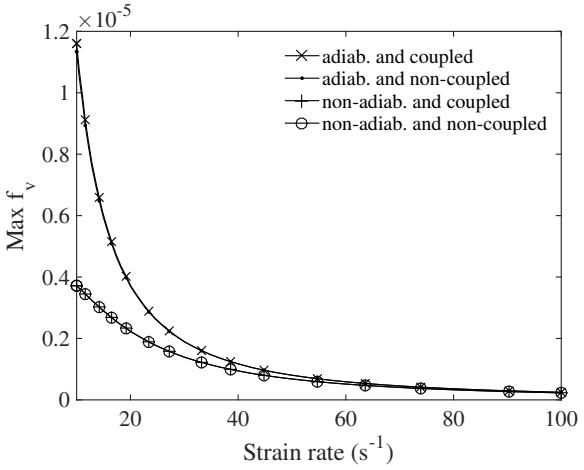


Figure 6: Maximum soot volume fraction for different strain rates

between the two phases is accounted for. A difference of more than 1% in the adiabatic case is found for $a = 25\ s^{-1}$. At this strain rate the value of $Y_S$ is 0.0145. The difference slowly increases as the amount of soot increases until a difference of 2.5%, for the lower strain rate. It is not found a difference of more than 1% in the non adiabatic case. This result means that the $Y_S$ is not sensitive to the small changes in the temperature and in the gas mixture composition caused by the soot formation in the present conditions.

For soot volume fraction similar result is obtained, see Fig. 6. A difference of more than 1% in the adiabatic case is found for $a = 20\ s^{-1}$. At this strain rate the value of $f_v$ is 3.6 $ppm$ and $Y_S = 2\%$. The difference slowly increases as the amount of soot increases until $\Delta f_v = 0.26\ ppm$ in the lower strain rate, a difference of 2.3%. Is not found a difference of more than 1% in the non adiabatic case.

The results presented above show that for predicting flame temperature and soot production, the interaction between the two phases should be accounted for at relatively high temperatures and significant soot volume fractions ($Y_S > 2\%$ and $f_v > 3.6ppm$). In the present work, these conditions are found for the adiabatic case and for strain rates lower than 20 $s^{-1}$. The results indicate that the lower the strain rate the higher the coupling importance.

The gas-phase species related to soot formation and oxidation are also investigated. It has been found that all species related to soot are affected, specially in the higher temperature condition (adiabatic case). Here only the species responsible for soot nucleation and surface growth, $C_2H_2$, and the gas-phase product of these reactions, $H_2$, are presented. In Fig. 7 and 8 the maximum $C_2H_2$ and $H_2$ mass fractions are presented respectively.

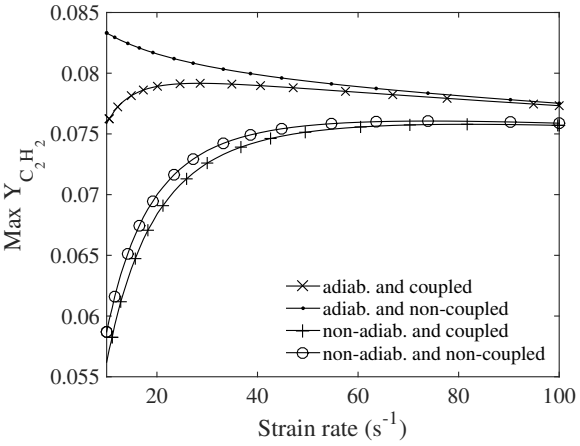


Figure 7: Maximum $C_2H_2$ mass fraction for different strain rates

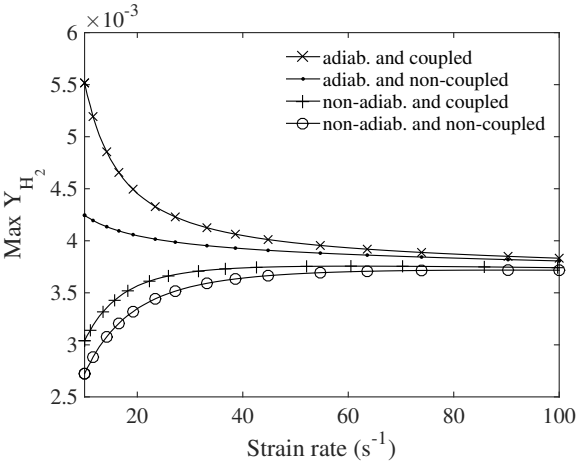


Figure 8: Maximum $H_2$ mass fraction for different strain rates

As seen in Fig. 7 the difference between coupled and non coupled cases varies from small differences (0.2%) for adiabatic and non-adiabatic cases for $a = 100\ s^{-1}$ to significant differences (8.9%) for adiabatic and (4.2%) non-adiabatic cases for 10 $s^{-1}$, with the non-coupled cases presenting higher amount of $C_2H_2$. These results are expected, since $C_2H_2$ is not consumed in soot nucleation and surface growth reactions for the non-coupled cases. Note also that for the adiabatic non-coupled case, the $C_2H_2$ concentration always increases as the strain rate is reduced due to the increase in soot produc-

tion. In the non-adiabatic case, the flame temperature is significantly reduced due to radiant heat losses which in turn reduces the $C_2H_2$ and soot production. With heat losses the difference between the coupled and non-coupled cases is lower. This result confirms that, for the present conditions, the thermal coupling through radiation losses is more important than the mass coupling, since the soot model is more sensitive to the temperature than the $C_2H_2$ concentration.

In Fig. 8 is shown the maximum hydrogen mass fraction. The difference between coupled and non-coupled cases varies from small differences (0.7%) for adiabatic and non-adiabatic cases for higher strain rates (100 $s^{-1}$) to large differences (29.9%) for adiabatic and (11.6%) non-adiabatic cases for lower strain rates (10 $s^{-1}$). Thus, $H_2$ is more sensitive to soot formation then acetylene through reactions $R_1$ and $R_2$. A consequence of this result is that, since $H_2$ diffuses faster than the other species, the production of soot may imply an increase of preferential diffusion effects.

## Conclusions

In this work a numerical model is developed aiming at investigating soot formation in different conditions for an ethylene counterflow diffusion flame. In order to access modeling limitations the mass and energy coupling between soot solid particles and gas-phase species are investigated. A semi-empirical two equation model is chosen for predicting soot mass fraction and number density. The model describes particle nucleation, surface growth and oxidation. For the gas-phase a detailed kinetic mechanism is considered (GRI 3.0). Additionally the effect of considering gas and soot radiation heat losses is evaluated in the optically thin limit approximation. Simulations were done for pure ethylene/air counterflow flames at atmospheric pressure for a range of conditions that produce low to significant amounts of soot. To achieve these conditions the strain rate, $a$, applied at the oxidizer side, was varied from 100 to 10 $s^{-1}$.

The results presented above show that for predicting flame temperature and soot production, the interaction between the two phases should be accounted for at relatively high temperatures and significant soot volume fractions ($Y_S > 2\%$ and $f_v > 3.6ppm$). In the present work, these conditions are found for the adiabatic case and for strain rates lower than 20 $s^{-1}$. The results indicate that the lower the strain rate the higher the coupling importance.

Significant changes were observed in the gas-phase species related to soot formation and oxidation, i.e., $C_2H_2$, $H_2$, $CO$, $H$, $O_2$, $OH$ and $O$, specially in the adiabatic cases, since higher temperatures results in significant amount of soot produced for lower strain rates. In the non-adiabatic cases the differences between the coupled and non-coupled were smaller. In these cases, where the temperature and $Y_S$ are lower, the soot formation and consumption does not considerably change the system composition.

Thus, for similar flame conditions to the ones treated here, it is important to take into account the interactions between the solid particles and gas-phase species. This is particularly important for preferential diffusion problems and detailed soot models which depend on complex chemistry to capture numerous PAHs. For simulations where the goal is to analyze only global parameters as flame temperature and soot volume fraction, the mass and energy coupling between the two phases can be neglected, but radiant heat losses should be accounted for.

## Acknowledgments

The first author acknowledges the financial support of the CAPES under Project No. BEX5381-13-4.

## References

[1] F. Liu, H. Guo, G. J. Smallwood, O. L. Gulder, Journal of Quantitative Spectroscopy and Radiative Transfer 73 (2002) 409 – 421.
[2] I. M. Kennedy, Progress in Energy and Combustion Science 23 (1997) 95 – 132.
[3] J. Moss, C. Stewart, K. Young, Combustion and Flame 101 (1995) 491 – 500.
[4] A. D'Anna, J. Kent, Combustion and Flame 144 (2006) 249 – 260.
[5] F. Liu, H. Guo, G. J. Smallwood, M. E. Hafi, Journal of Quantitative Spectroscopy and Radiative Transfer 84 (2004) 501 – 511.
[6] M. R. Charest, Ö. L. Gülder, C. P. Groth, Combustion and Flame 161 (2014) 2678 – 2691.
[7] M. R. Charest, C. P. Groth, Ö. L. Gülder, Combustion Theory and Modelling 14 (2010) 793–825.
[8] R. Mehta, D. Haworth, M. Modest, Proceedings of the Combustion Institute 32 (2009) 1327 – 1334.
[9] D. Carbonell, A. Oliva, C. Perez-Segarra, Combustion and Flame 156 (2009) 621 – 632.
[10] K. Leung, R. Lindstedt, W. Jones, Combustion and Flame 87 (1991) 289 – 305.
[11] L. P. H. de Goey, J. H. M. ten Thije Boonkkamp, Combustion and Flame 119 (1999) 253–271.
[12] M. Fairweather, W. Jones, R. Lindstedt, Combustion and Flame 89 (1992) 45 – 63.
[13] Q. Zhang, H. Guo, F. Liu, G. J. Smallwood, M. J. Thomson, Combustion Theory and Modelling 12 (2008) 621–641.
[14] I. M. Kennedy, W. Kollmann, J.-Y. Chen, Combustion and Flame 81 (1990) 73 – 85.
[15] J. Nagle, R. Strickland-Constable, in: Proceedings of the fifth conference on carbon, volume 1, The MacMillan Co., pp. 154–164.
[16] D. Bradley, G. Dixon-Lewis, S. E. din Habik, E. Mushi, Symposium (International) on Combustion 20 (1984) 931 – 940.
[17] O. Ezekoye, Z. Zhang, Combustion and Flame 110 (1997) 127 – 139.
[18] M. Smooke, C. McEnally, L. Pfefferle, R. Hall, M. Colket, Combustion and Flame 117 (1999) 117 – 139.
[19] J. Chen, Y. Liu, B. Rogg, in: N. Peters, B. Rogg (Eds.), Reduced Kinetic Mechanisms for Applications in Combustion Systems, volume 15, Springer, 1993, pp. 196–223.
[20] W. Grosshandler, Nist technical note 1402, 1993.
[21] M. W. Chase Jr., Journal of Physical and Chemical Reference Data Fourth Edition (1998).
[22] CHEM1D, One-dimensional laminar flame code, Eindhoven Technological University, n.d.
[23] C. Wilke, The journal of chemical physics 18 (1950) 517–519.
[24] S. Mathur, P. Tondon, S. Saxena, Molecular physics 12 (1967) 569–579.